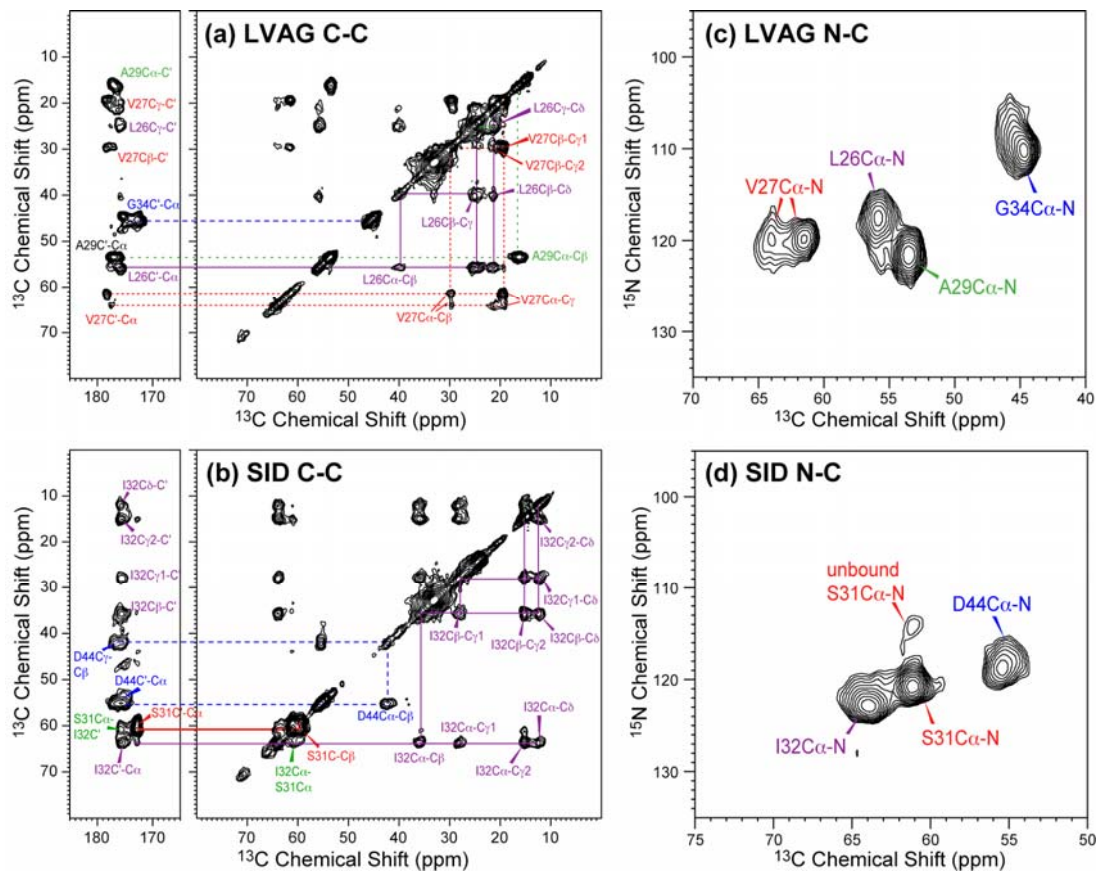


Contents

- (A) Chemical shift assignment of amantadine-bound M2 in DMPC bilayers
- (B) Additional ^{13}C - ^2H REDOR spectra, REDOR simulation protocol and model compound result
- (C) REDOR simulations for various M2 structural models
- (D) Computation procedure for the structure ensemble of amantadine-bound M2 in lipid bilayers
- (E) Synthesis of perdeuterated amantadine
- (F) Complete set of ^2H spectra of perdeuterated amantadine in lipid bilayers

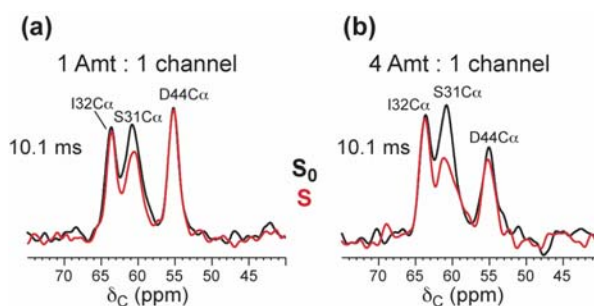
(A) Chemical shift assignment of amantadine-bound M2 in DMPC bilayers.

Supplementary Figure S1. 2D ^{13}C - ^{13}C and ^{15}N - ^{13}C correlation spectra of amantadine-bound M2(22-46) in DMPC bilayers for chemical shift assignment. (a) 2D DARR spectrum of LVAG-M2 (L26, Val27, A29, and Gly34 labels) with 40 ms mixing. (b) 2D DARR spectrum of SID-M2 (S31, I32 and D44 labels) with 40 ms mixing. (c) 2D ^{15}N - ^{13}C correlation spectrum of LVAG-M2. (d) 2D ^{15}N - ^{13}C correlation spectrum of SID-M2. All spectra were measured at 243 K under 7 kHz MAS.

Supplementary Table S1. ^{13}C and ^{15}N isotropic chemical shifts of amantadine-bound M2(22-46) in DMPC bilayers. ^{13}C chemical shifts are referenced to $\alpha\text{-Gly } ^{13}\text{CO}$ (176.4 ppm) on the TMS scale and ^{15}N chemical shifts are referenced to ^{15}N -acetylvaline (122.0 ppm) on the NH_3 scale.

Residue	Site	δ (ppm)	Residue	Site	δ (ppm)	
L26	N	117.5	Ser31	N	120.8s, 114.1w	
	C'	176.3		C'	172.8	
	C α	55.8		C α	61.0	
	Val27	C β	39.5	I32	C β	59.5
		C γ	25.1		N	122.8
		C δ 1	24.2		C'	175.6
		C δ 2	21.2		C α	64.0
N		119.8	C β		35.9	
C'		178.3s, 177.5w	C γ 1		28.2	
C α		61.4s, 64.2w	C γ 2		15.2	
A29	C β	29.6	Gly34	C δ	12.4	
	C γ 1	21.2		N	110.2	
	C γ 2	19.3		C'	175.1	
	A29	N	121.6	D44	C α	44.9
		C'	177.0		N	118.7
		C α	53.4		C'	175.7
		C β	16.2		C α	55.6
			C β	42.4		

(B) Additional ^{13}C - ^2H REDOR spectra, REDOR simulation details and model compound result



Supplementary Figure S2. Double-quantum filtered $^{13}\text{C}\{^2\text{H}\}$ REDOR spectra of amantadine-bound M2 in DMPC bilayers. As shown before¹, the experiment incorporates a SPC5 dipolar recoupling sequence² before the REDOR period to generate ^{13}C - ^{13}C double-quantum coherences, which suppress all natural abundance ^{13}C signals of the lipids in the spectra. The experiments were carried out at 243 K under 4750 Hz MAS. (a) SID-M2 spectra at Amt/P = 1:4, corresponding to a stoichiometric amount of Amt per channel. The D44 C α signal shows no dephasing. (b) SID-M2 spectra at Amt/P = 4:4, corresponding to 4-fold excess Amt to channel. D44 C α is now dephased to a small extent, indicating that the excess amantadine binds to the C-terminus near D44. Ser31 C α is dephased significantly at both amantadine concentrations, thus it is the high-affinity binding site.

^{13}C - ^2H REDOR simulations. The dephasing of a ^{13}C spin in the peptide by the recoupled dipolar fields of 12 equatorial deuterons on the amantadine molecule was simulated in detail by considering the uniaxial rotation of amantadine. The coupling of ^{13}C to 15 deuterons increases the second moment (i.e. the sum of the squares) of the ^{13}C - ^2H dipolar couplings 15-fold compared to a single ^{13}C - ^2H spin pair, thus speeding up the dephasing by a factor of $\sqrt{15} \approx 3.9$.

The three axial deuterons have a three times wider spectrum, which makes their inversion significantly incomplete under the ^2H 90° pulse length of $6.2 \mu\text{s}$. Thus, they were neglected in the simulations.

The inversion efficiency of the 12 deuterons was about 70%, as determined by measurements on Ala- CD_3 (Supplementary Figure S3), which has a very similar motionally narrowed ^2H spectrum to amantadine.

The geometry of the 12 equatorial amantadine deuterons is as follows. Six deuterons are located on one ring of 2.20 \AA radius centered on the C-N bond axis. The other six deuterons lie on two rings of 2.48 \AA radius that are so close (separated by only 0.37 \AA) that they were combined into one ring. The planes of the two rings are separated by 2.10 \AA along the C-N axis.

The orientation-dependent ^{13}C - ^2H REDOR frequency (ω_{CD}) under MAS is

$$\omega_{CD}(\beta, \gamma, r) = \delta_{CD}(r) \cdot \frac{\sqrt{2}}{\pi} \cdot \sin 2\beta \sin \gamma, \quad (1)$$

where β is the polar angle between the C-D vector and the rotor axis and γ is the azimuthal angle of the internuclear vector around the rotor axis. The coupling constant δ_{CD} depends on the ^{13}C - ^2H distance r according to:

$$\delta_{CD}(r) = -2 \cdot \frac{\mu_0}{4\pi} \hbar \frac{\gamma_C \gamma_D}{r^3} = -2\pi \cdot 9.3 \text{ kHz} \frac{1}{(r/1 \text{ \AA})^3} \quad (2)$$

The ω_{CD} values were calculated for β , γ and r values that correspond to various locations of the deuterons on each ring, which are sampled at 10° steps around the channel axis. Since each ring undergoes uniaxial rotation, the REDOR frequencies were then averaged to give $\bar{\omega}_{CD}$.

For ^{13}C coupled to an $I = 1$ spin of a deuteron, the $2I + 1 = 3$ allowed values of the z -component of the deuterium spin angular momentum result in three equally spaced spectral lines of equal intensity, at 0 and $\pm \bar{\omega}_{CD}$, for each orientation of the C-D vector. Thus, the single spin-pair ^{13}C - ^2H REDOR time signal after N rotor periods, t_r , for one channel orientation is:

$$(S/S_0)_{\text{single spin pair}} = [1 + 2 \cos(\bar{\omega}_{CD} N t_r)]/3. \quad (3)$$

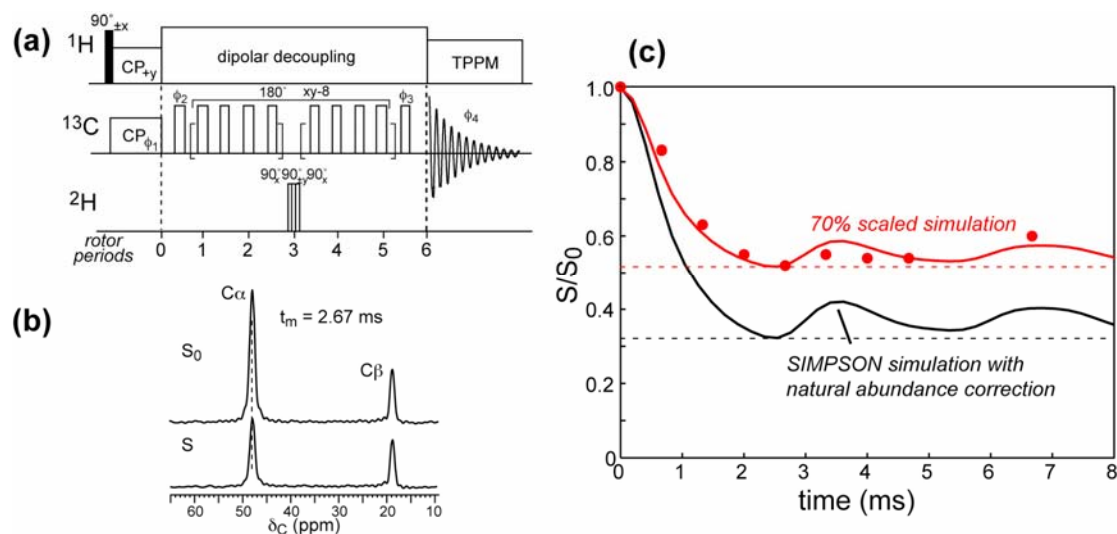
For M deuterons, the REDOR time signal is the product of the single-spin-pair signals,

$$(S/S_0)_{M \text{ spin pairs}} = \frac{1}{3^M} \prod_{m=1}^M [1 + 2 \cos(\bar{\omega}_{CD,m} N t_r)] \quad (4)$$

Due to the fast rotation of the amantadine molecule around the C-N axis, all six deuterons on each ring have the same motionally averaged ^{13}C - ^2H dipolar coupling. Thus, the motionally averaged REDOR frequencies for each ring, $\bar{\omega}_{CD}^A$ and $\bar{\omega}_{CD}^B$, are multiplied to give the total REDOR signal experienced by each peptide ^{13}C :

$$(S/S_0)_{12 \text{ amantadine deuterons}} = \frac{1}{3^{12}} \left\langle \left[1 + 2 \cos(\bar{\omega}_{CD}^A N t_r) \right]^6 \cdot \left[1 + 2 \cos(\bar{\omega}_{CD}^B N t_r) \right]^6 \right\rangle \quad (5)$$

This REDOR signal is finally powder averaged for all channel orientations relative to the rotor axis. Powder averaging was performed in a molecule- (peptide-) fixed frame, by sweeping the rotor-axis orientation over the surface of a unit sphere and by rotation around the rotor axis, each in 10° steps.



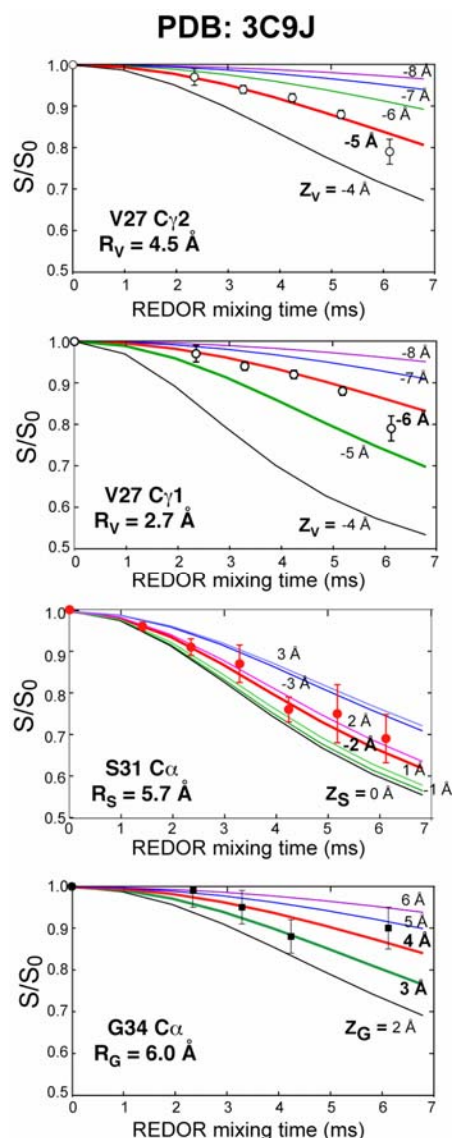
Supplementary Figure S3. ^{13}C - ^2H REDOR data of $^{13}\text{C}\alpha$, 3,3,3- $^2\text{H}\beta$ labeled alanine for determining the amplitude scaling of the single- ^2H -pulse REDOR experiment.

(a) The REDOR pulse sequence contains a single ^2H composite π pulse ($90^\circ_{90^\circ, 90^\circ}$) of 18.6 μs in the middle of the mixing period, and multiple ^{13}C π pulses of 10 μs spaced half a rotor period apart. The phase cycles are: $\phi_1 = +x +x +y +y -x -x -y -y$; $\phi_2 = \phi_1, \phi_1 + 90^\circ, \phi_1 + 180^\circ, \phi_1 + 270^\circ$; $\phi_3 = R, R + 90^\circ, R + 180^\circ, R + 270^\circ$, where R is a 32-step cycle of ($\phi_1 + 90^\circ, \phi_1 + 180^\circ, \phi_1 + 270^\circ, \phi_1$); The receiver phase $\phi_4 = Q, Q, Q, Q, -Q, -Q, -Q, -Q$, where $Q = +x -x +y -y -x +x -y +y$.

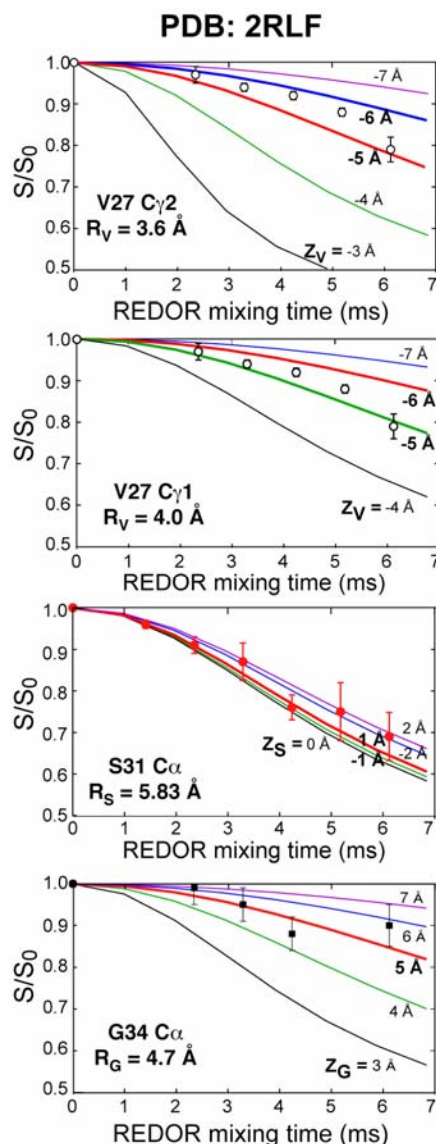
(b) Representative REDOR control (S_0) and dephased (S) spectra of $^{13}\text{C}\alpha$, 3,3,3- $^2\text{H}\beta$ labeled alanine diluted in unlabeled alanine at a 1:9 ratio. The spectra were measured at a MAS frequency of 4.250 kHz. The $\text{C}\alpha$ signal experiences significant dephasing to the three intramolecular methyl deuterons, whereas the $\text{C}\beta$ signal mostly (90%) results from ^2H -unlabeled alanine without any significant dephasing.

(c) REDOR S/S_0 values (circles) and simulations (solid lines). Black line is the SIMPSON simulation³ for an ideal δ -function ^2H pulse, which completely inverts the ^2H quadrupolar spectra. The motionally averaged $^{13}\text{C}\alpha$ - $^2\text{H}\beta$ dipolar coupling is 364 Hz for each of the three $^{13}\text{C}\alpha$ - $^2\text{H}\beta$ spin pairs based on the crystal structure $\text{C}\alpha$ - $\text{H}\beta$ distance of 2.04 \AA ⁴. The simulation curves have been corrected for the natural abundance $^{13}\text{C}\alpha$ intensity. The time point for the first REDOR minimum from the simulation is very similar to that of the experimental data, verifying that this single ^2H -pulse REDOR experiment does not slow down dipolar evolution⁵. The effects of incomplete inversion of the ^2H spectrum and the imperfection of the ^2H pulse is manifested as a 70% scaling of the theoretical maximum dephasing to the measured dephasing. This scaling factor is used for all simulated M2-amantadine REDOR time signals.

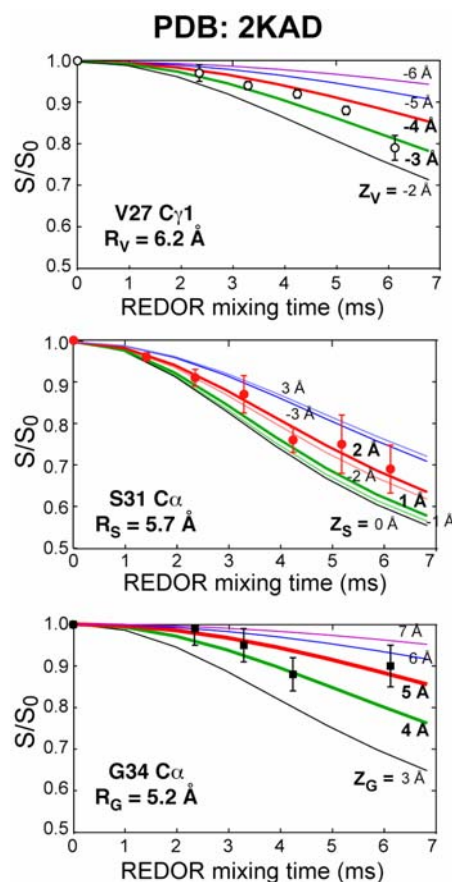
(C) REDOR simulations for various M2 structural models



Supplementary Figure S4. Simulations of Val27 C γ 1, Ser31 C α and Gly34 C α $^{13}\text{C}\{^2\text{H}\}$ REDOR data using the pore sizes of the low-pH crystal structure of amantadine-bound M2(22-46) (PDB code: 3C9J)⁶. Val27 C γ 1 has a best-fit Z_V of -6 \AA while the Gly34 C α best-fit Z_G is 3.5 \AA . Ser31 C α has a best-fit Z of 2 \AA or -2 \AA . Either Z_S value agrees only marginally with the Val27 C γ 1 – Ser31 C α plane separation (4.8 \AA) and the Ser31 C α - Gly34 C α plane separation (4.6 \AA) in the model. Thus, the low-pH structure of Amt-bound M2 in detergent is different, as expected, from the high-pH SSNMR structure of bound M2 in lipid bilayers.

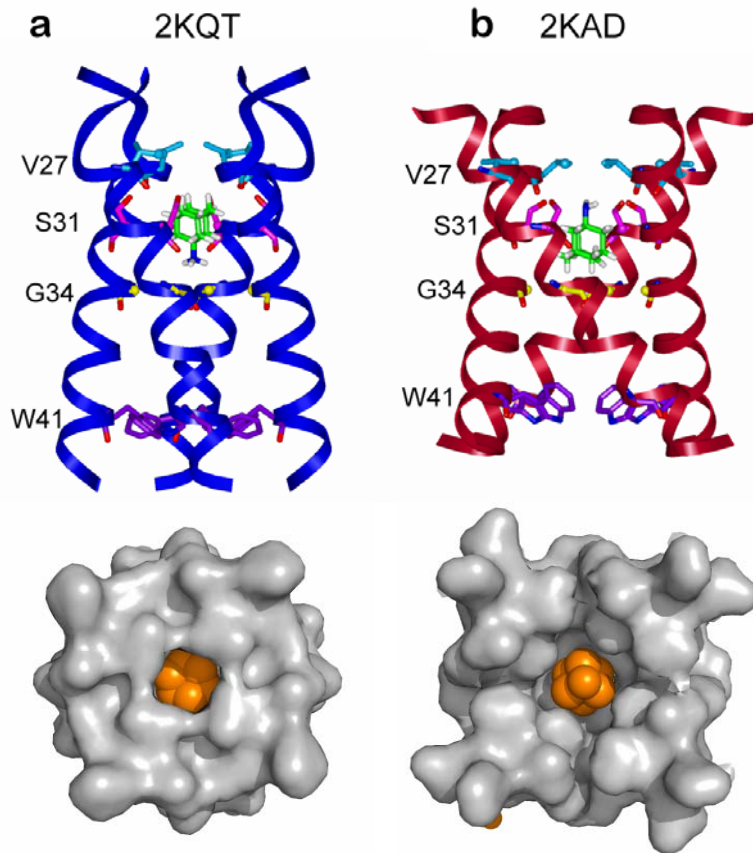


Supplementary Figure S5. Simulations of Val27 C γ 1, Ser31 C α and Gly34 C α $^{13}\text{C}\{^2\text{H}\}$ REDOR data using the pore sizes of the solution NMR structure of DHPC micelle-bound M2(18-60) (PDB code: 2RLF)⁷. The two Val27 C γ carbons have similar R values in this structural model. The 19.5-ppm Val27 C γ signal in the REDOR spectra has been recently stereospecifically assigned to C γ 1⁸. To be complete, the pore radii of both C γ 1 and C γ 2 in the solution NMR structure were used in the REDOR simulation. For the C γ 2 radius of 3.6 \AA , the best-fit Z_V of $-5.7 \text{ \AA} \pm 0.5 \text{ \AA}$ combined with the Gly 34 best fit Z_G of $5.0 \pm 0.5 \text{ \AA}$ gives a Val27 C γ 2-Gly34 C α height difference of 10.7 \AA , which is incompatible with the plane separation of 12.2 \AA in the structure. However, the Val27 C γ 1 best-fit Z_V value of $-5.5 \pm 0.3 \text{ \AA}$, combined with the Ser31 and Gly34 best fits, is a consistent solution.



Supplementary Figure S6. Simulations of Val27 C γ 1, Ser31 C α and Gly34 C α $^{13}\text{C}\{^2\text{H}\}$ REDOR data using the pore sizes of the DLPC bilayer-bound M2(22-46) structure (PDB code: 2KAD) obtained from SSNMR⁹. The best-fit Z_V , using the Val27 C γ 1 pore radius of 6.2 Å in the structure, is -3.5 Å. The best-fit Z_G for Gly34 C α is 4.5 ± 0.5 Å. The resulting Val27-Gly34 height difference of 8.0 Å is significantly smaller than the 9.5 Å plane separation in the model. Thus, this model is not consistent with the M2-amantadine distance results.

The DMPC-bound M2(22-46) structure model (PDB: 1NYJ) obtained from oriented-sample SSNMR experiments¹⁰ is similar to the 2KAD model. Thus it is also not compatible with the REDOR distance constraints. In the 1NYJ model, the Val27 C γ 1 pore radius is even larger (7.3 Å), which would result in an even shorter Z_V .



Supplementary Figure S7. Comparison of SSNMR structures of M2 in lipid bilayers determined with and without protein-amantadine distances. **a.** Current structure restrained by protein-drug distances (PDB: 2KQT). The side view shows the closest contact between amantadine and Ser 31 (magenta). The N-terminal top view shows that the drug is tightly enclosed in the protein. **b.** Structural model restrained by ^{13}C , ^{15}N chemical shifts and three inter-helical distances but no protein-drug distances (PDB: 2KAD). The drug location in the picture is hypothetical⁹. The N-terminal view shows a more solvent-accessible binding pocket. The ribbon diagrams were generated using Insight II and the space-filling models were generated using PyMOL.

Supplementary Table S2. ^{13}C - ^2H M2-Amt distances from REDOR measurements.

Planes	Plane separations (Å)	Uncertainty
V27 C γ 1 – S31 C α	5.3 Å	± 0.5 Å
S31 C α - G34 C α	5.0 Å	± 0.5 Å
V27 C γ 1 – G34 C α	10.3 Å	± 1.0 Å
Carbons	Pore radius (Å)	Uncertainty
V27 C γ 1	3.8 Å	± 0.5 Å
S31 C α	5.9 Å	-0.2 Å, +0.4 Å
G34 C α	4.9 Å	± 0.5 Å

(D) Computation procedure for the SSNMR structure ensemble of amantadine-bound M2 in lipid bilayers

An ideal helix with the sequence SSDPLVVAASIIGILHLILWILDRL was constructed using standard internal geometry and by setting the (ϕ, ψ) values to $(-65^\circ, -42^\circ)$. Side chain rotamer conformations were taken from the high-resolution M2 crystal structure (PDB ID: 3BKD). The ideal helix was then split at the Gly34-Ile35 amide bond to generate two separate helices. Each helix fragment was then transformed to the global frame of reference such that the helical axes were coincident with the global Z axis. The Gly34-Ile35 bond was then rebuilt using a rigid-body optimization procedure composed of a harmonic potential to optimize the internal geometry between Gly34-Ile35, and a harmonic potential to optimize the fit to the ^{15}N - ^1H dipolar couplings from SSNMR¹¹. To simplify coordinate transformation, Gly34 C α was set as at the origin. The rigid-body optimization procedure resulted in a helix that agreed with the N-H bond orientations to within $\pm 10^\circ$ of the previous SSNMR results.

To maximize agreement with the ^{15}N orientational constraints further, an inverse kinematics algorithm (IKA) was used to gradually relax the backbone¹². To reduce large-scale movements between the N-terminal and C-terminal segments of the helix, the wriggling algorithm was used to construct a set of suitably local dihedral-angle moves along the protein chain without distorting the internal bond lengths and bond angles. The stochastic nature of this algorithm allowed us to easily integrate in a Monte Carlo/simulated annealing (MC/SA) minimization strategy. Thus, small random perturbations to the (ϕ, ψ) angles (up to $\pm 1^\circ$) were introduced along the backbone of the helix subject to the following potential:

$$V = \sum_i^{\text{radial}} C_I \cdot (r_i - r_0)^2 + \sum_i^{\text{dipolar}} C_{II} \cdot (\theta_i - \theta_0)^2 + \sum_i^{\text{dihedral}} C_{III} \cdot (\tau_i - \tau_0)^2 + \sum_i^{\text{dist}} C_{IV} \cdot (d_i - d_0)^2 + \sum_i \sum_{i>j}^{\text{nonb}} \left(\frac{A}{R^{12}} - \frac{B}{R^6} \right)$$

The temperature was initially set to 10^6 K and decreased by 10% every 100 steps until a temperature of 25 K was reached. The constants (C_I - C_{IV}) were obtained through a trial-and-error process. Some side chain rotamers were changed to maximize agreement with the radial distances (Supplementary Table 2). An ensemble of models was obtained by selecting the top scoring model after one round of MC/SA minimization and refining again with the IKA. The constant C_{III} was set to 50 kcal/mol-radian². Since the radial distance provided excellent restraints between the drug and M2, we were able to position the amantadine molecule near S31 without the need for further minimization.

A brief description for each of the terms in the above potential energy function is provided below:

1) Radial potential—used to improve the fit between the distance belonging to atoms in Supplementary Table S2 and the channel axis (i.e., the global Z axis). The constant C_I was set to 1000 kcal/mol- \AA^2 .

2) Dipolar angle potential—used to improve the fit with the ^{15}N dipolar coupling data measured by SSNMR (PDB ID: 2H95) (Supplementary Table S3)¹¹. The angle θ is measured between the

channel axis and the bond vector formed between the amide backbone nitrogen and the corresponding amide hydrogen. The constant C_{II} was set to 1000 kcal/mol-radians².

3) Dihedral potential—used to maintain the helical geometry by forcing the dihedral angles to stay in an acceptable region of Ramachandran space. The constant C_{III} was set to 100 kcal/mol-radians². The starting dihedral angle value was set as the target value.

4) Distance potential—used to maintain the helical geometry by forcing the hydrogen bond distances between the backbone of the i^{th} carbonyl-oxygen and $i+4^{\text{th}}$ nitrogen to remain close to the starting value. This potential was also used to restrain the Trp41 distance in Supplementary Table S4. The constant C_{IV} was set to 100 kcal/mol-Å².

5) Lennard-Jones potential—the parameters for this potential were taken directly from the CHARMM22 force field parameter file in XPLOR-NIH¹³. Interactions between the i^{th} and $i+4^{\text{th}}$ bonded neighbor interactions were not considered and non-bonded cutoffs were not utilized. After each pass of the local sampling algorithm, a C4 operation about the channel axis was performed to generate the four equivalent chains before calculating the energy.

Supplementary Table S3. N-H vector angles with respect to the channel axis used to restrain the current structure. The angles are based on ^{15}N SSNMR data of M2 in DMPC bilayers at high pH with amantadine bound (PDB: 2H95)¹¹.

Residue	Angle (°)	Residue	Angle (°)
V27	17.2	H37	NA
V28	40.1	L38	12.0
A29	43.5	I39	31.5
A30	29.8	L40	32.7
S31	26.4	W41	9.74
I32	44.1	I42	15.5
I33	36.1	L43	43.0
G34	15.5	D44	17.2
I35	31.5	R45	40.1
L36	32.1	L46	43.5

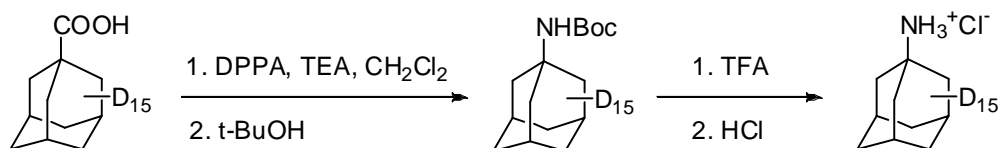
Supplementary Table S4. Additional restraints for M2 structure calculation.

Residue	χ_1 angles	Uncertainty
V27	+158° or -158°	±4°
V28	+158° or -158°	±4°
Residue	Diagonal distance	Uncertainty
W41 5- ^{19}F (Hz3)	16.5 Å	±0.8 Å

(E) Synthesis of perdeuterated amantadine

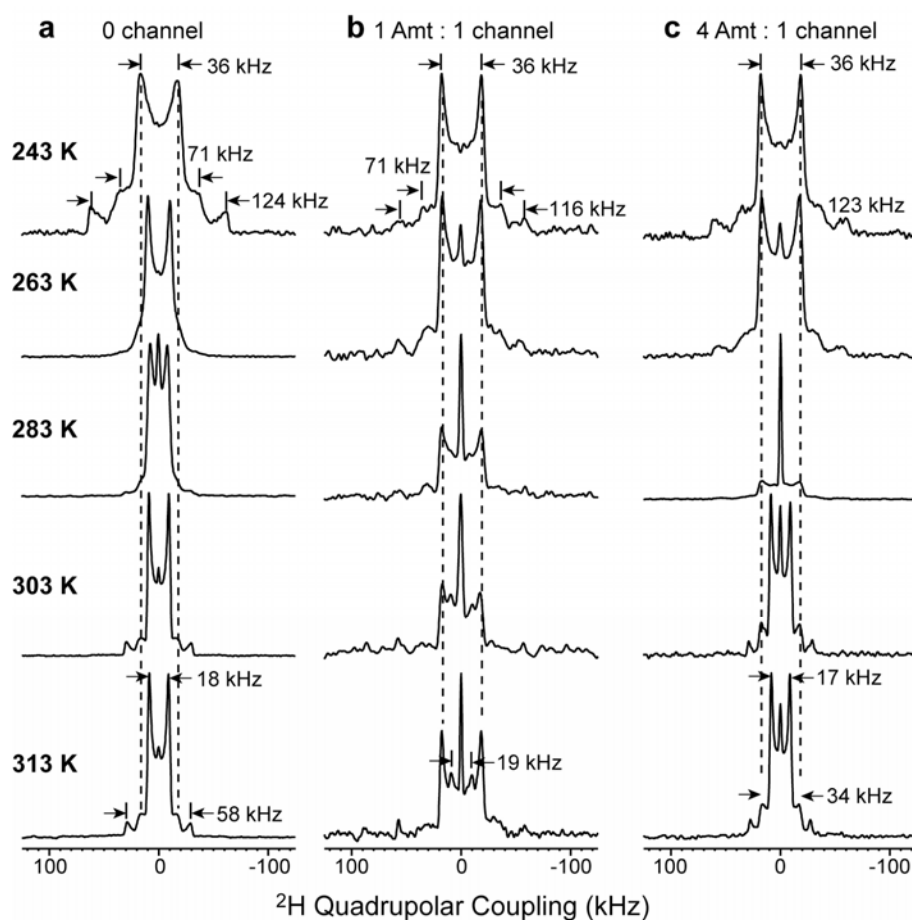
All chemicals were purchased from commercial vendors and used without further purification unless otherwise noted. 1-adamantane-d₁₅-carboxylic acid was purchased from C/D/N isotopes Inc. ¹³C NMR spectra were recorded on a DMX-360 NMR spectrometer. Chemical shifts are reported in parts per million (ppm) and referenced to the residual solvent (CD₃OD) signal at 49.15 ppm. The following abbreviations were used in reporting the NMR spectra: s: singlet, p: pentet.

All reactions were carried out under a N₂ atmosphere unless otherwise stated. HPLC grade solvents were used for all reactions. Column chromatography was performed using silica gel (230-400 mesh). Low-resolution mass spectra were obtained using an ESI technique on 3200 Q Trap LC/MS/MS system (Applied Biosystem).



Scheme 1: 1-aminoadamantane-d₁₅-hydrochloride ¹⁴.

Diphenylphosphorylazide (DPPA) (1.29 ml, 6 mmol) and triethylamine (0.84 ml, 6 mmol) were added to a solution of 1-adamantane-d₁₅-carboxylic acid (0.98 g, 5 mmol) in 10 ml CH₂Cl₂ at ambient temperature. The reaction was stirred for 2 hours. An additional 10 ml CH₂Cl₂ and 10 ml H₂O were added to the reaction mixture, the organic layer was separated and washed sequentially with H₂O, saturated NaHCO₃ and brine and dried over MgSO₄. Solvent was removed by rotary evaporation and t-BuOH (50 ml) was added. The solution was heated to reflux under N₂ atmosphere for 5 hours. Excess t-BuOH was removed in vacuo and the residue was treated with 50% TFA/CH₂Cl₂ at ambient temperature for 2 hours. N₂ was purged through the mixture to remove excess TFA and CH₂Cl₂ to give yellow oil. 4M HCl in dioxane (3 ml) was added and the mixture was added dropwise to cold diethyl ether. A white solid was collected by centrifugation and subsequent decanting of the ether supernatant. Further flash column chromatography purification gave 1-aminoadamantane-d₁₅-hydrochloride as a white power (0.83 g, Yield: 82%). ¹³C NMR (90 MHz, CD₃OD) gave signals at 52.62 ppm (s), 40.51 ppm (p, *J* = 18.9 Hz), 35.11 ppm (p, *J* = 20.7 Hz), and 29.47 ppm (t, *J* = 21.6 Hz). The calculated mass for C₁₀H₂ND₁₅ (M + H)⁺ is 167.3, and the measured value by ESI-MS was 167.2.

(F) Complete set of ^2H spectra of perdeuterated amantadine in lipid bilayers.

Supplementary Figure S8. Variable-temperature ^2H spectra of perdeuterated amantadine in DMPC bilayers. **a.** Without any M2. **b.** With M2 at Amt/P = 1 : 4. **c.** With M2 at Amt/P = 4 : 4. The spectra were measured from 243 K to 313 K.

References

- 1 Su, Y., Doherty, T., Waring, A. J., Ruchala, P. & Hong, M. Roles of arginine and lysine residues in the translocation of a cell-penetrating peptide from (^{13}C) , (^{31}P) , and (^{19}F) solid-state NMR. *Biochemistry* **48**, 4587-4595 (2009).
- 2 Hohwy, M., Rienstra, C. M., Jaroniec, C. P. & Griffin, R. G. Fivefold symmetric homonuclear dipolar recoupling in rotating solids: application to double-quantum spectroscopy. *J. Chem. Phys.* **110**, 7983-7992 (1999).
- 3 Bak, M., Rasmussen, T. & Nielsen, N. C. SIMPSON: A General Simulation Program for Solid-State NMR Spectroscopy. *J. Magn. Reson.* **147**, 296-330 (2000).
- 4 Schmidt, A., Kowalewski, T. & Schaefer, J. Local packing in glassy polycarbonates by carbon-deuterium REDOR NMR. *Macromolecules* **26**, 1729-1733 (1993).
- 5 Sack, I. & Vega, S. Efficient deuterium-carbon REDOR NMR Spectroscopy. *J. Magn. Reson.* **145**, 52-61 (2000).
- 6 Stouffer, A. L. *et al.* Structural basis for the function and inhibition of an influenza virus proton channel. *Nature* **451**, 596-599 (2008).
- 7 Schnell, J. R. & Chou, J. J. Structure and mechanism of the M2 proton channel of influenza A virus. *Nature* **451**, 591-595 (2008).
- 8 Hong, M., Mishanina, T. V. & Cady, S. D. Accurate measurement of methyl ^{13}C chemical shifts by solid-state NMR for the determination of protein sidechain conformation: the influenza M2 transmembrane peptide as an example. *J. Am. Chem. Soc.* **131**, 7806-7816 (2009).
- 9 Cady, S. D., Mishanina, T. V. & Hong, M. Structure of amantadine-bound M2 transmembrane peptide of influenza A in lipid bilayers from magic-angle-spinning solid-state NMR: the role of Ser31 in amantadine binding. *J. Mol. Biol.* **385**, 1127-1141 (2009).
- 10 Nishimura, K., Kim, S., Zhang, L. & Cross, T. A. The closed state of a H^+ channel helical bundle combining precise orientational and distance restraints from solid state NMR. *Biochemistry* **41**, 13170-13177 (2002).
- 11 Hu, J. *et al.* Backbone structure of the amantadine-blocked transMembrane domain M2 proton channel from influenza A virus. *Biophys. J.* **92**, 4335-4343 (2007).
- 12 Cahill, S., Cahill, M. & Cahill, K. On the kinematics of protein folding. *J. Comput. Chem.* **24**, 1364-1370 (2003).
- 13 Schwieters, C. D., Kuszewski, J. J., Tjandra, N. & Clore, G. M. The Xplor-NIH NMR molecular structure determination package. *J. Magn. Reson.* **160**, 65-73 (2003).
- 14 Nasr, K., Pannier, N., Frangioni, J. V. & Maison, W. Rigid multivalent scaffolds based on adamantane. *J. Org. Chem.* **73**, 1056-1060 (2008).